

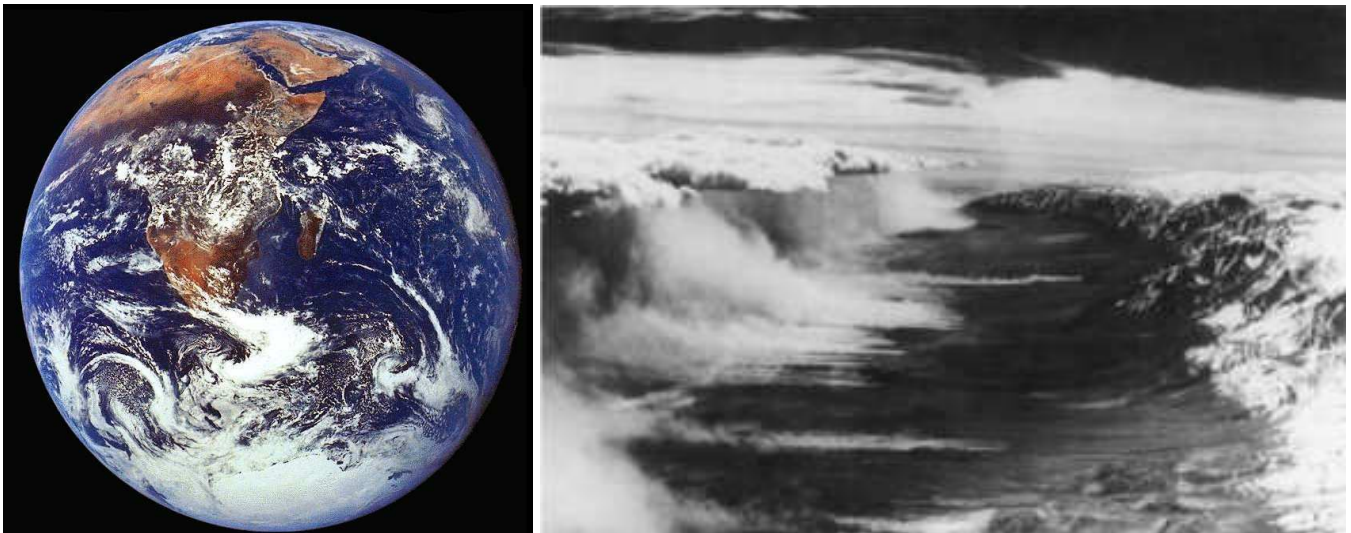
SIMULATION OF GEOPHYSICAL TURBULENCE: DYNAMIC GRID DEFORMATION

Piotr K Smolarkiewicz* and Joseph M Prusa†

*National Center for Atmospheric Research, Boulder, Colorado, U.S.A.

† Iowa State University, Ames, Iowa, U.S.A.

Motivation



- Geophysical turbulence embodies phenomena uncommon in engineering applications, such as breaking of internal inertia-gravity waves (viz. *localization*) and spans an enormous range of scales; e.g., $\kappa \sim \mathcal{O}(10^{20})$, for the Earth atmosphere.

- With mesh adaptivity for simulating complex geophysical flows in mind, we have developed a generalized mathematical framework for the implementation of deformable coordinates in a generic Eulerian/ semi-Lagrangian format of nonoscillatory-forward-in-time (NFT) schemes.

- There is more involved than a mere application of well-known mathematical theories. The apparatus of the Riemannian Geometry must be applied judiciously, in order to arrive at an effective numerical model.

3 Strategies for Prognostic Simulation

Geophysical turbulence is intermittent in nature. This dictates three viable simulation strategies:

- direct numerical simulation (DNS), with all relevant scales of motion resolved;
- large-eddy simulation (LES), with all relevant subgrid scales parameterized;
- implicit large-eddy simulation (ILES) — also known as very-large-eddy simulation (VLES), monotonically-integrated large-eddy-simulation (MILES), or implicit turbulence modeling — with a bohemian attitude toward subgrid scales.

- ILES a “do-nothing” approach that relies on nonoscillatory (physically-motivated) numerics that “adapts” itself to the flow in the course of a simulation \Leftrightarrow in progress and controversial, yet effective and relatively simple; i.e., practical.

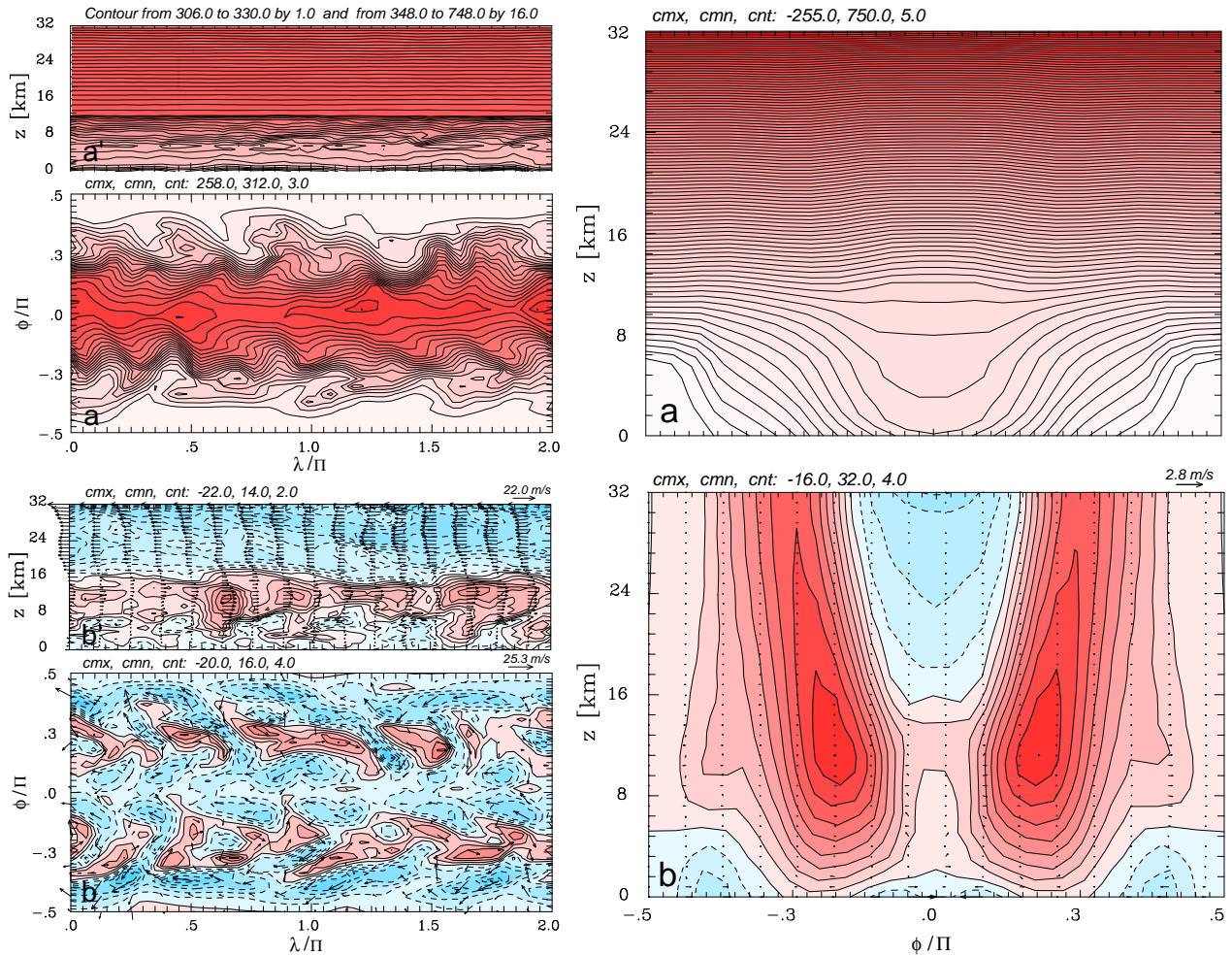


Figure 1: The idealized Held-Suarez climate problem; instantaneous solution after 3 years of simulation (left), and zonally averaged 3-year means (right).

RE: ILES Justification

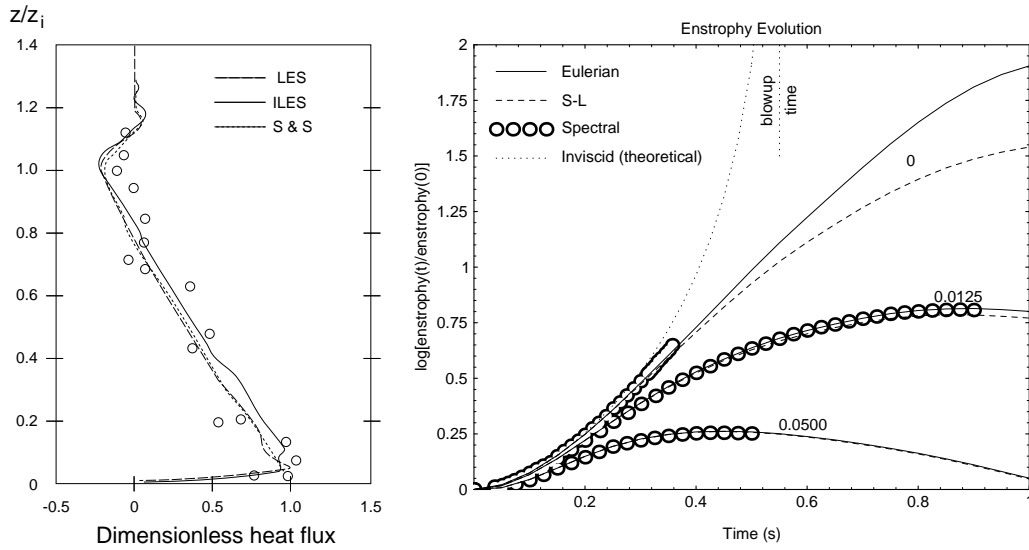


Figure 2: Left: LES/ILES of convective PBL, after Margolin et al. 1999.
Right: DNS/ILES of decaying turbulence, after Sm. & Prusa 2002.

$$\frac{\partial E(k, t)}{\partial t} = T(k, t) - 2\nu k^2 E(k) - \varepsilon_n(k, t) \Rightarrow \varepsilon_n := 2\nu_n k^2 E(k) \Rightarrow \nu_n(k)$$

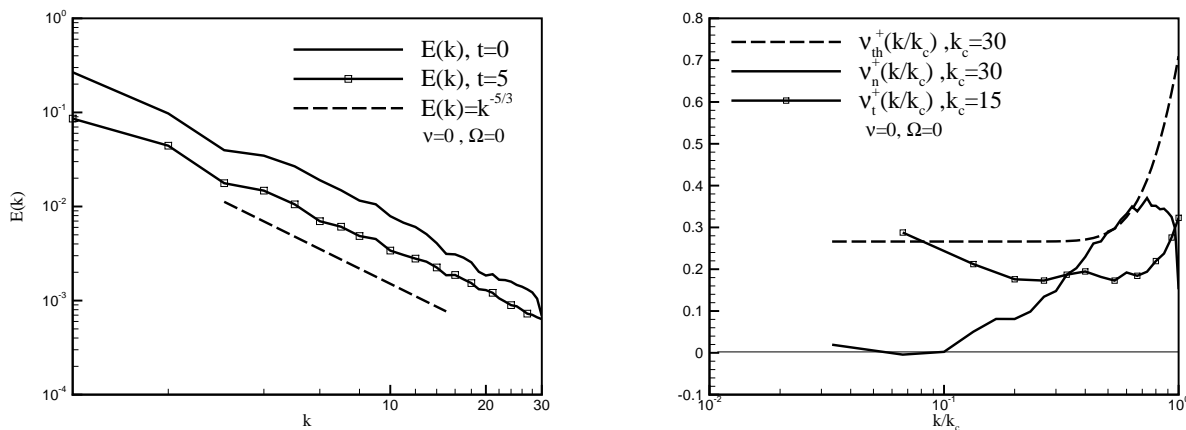


Figure 3: ILES of decaying turbulence, after Domaradzki et al. 2003.

- LES with physically-motivated SGS models \Leftrightarrow theoretically not universal enough, and practically much more complicated than ILES, but effective for shear-driven boundary layer flows.

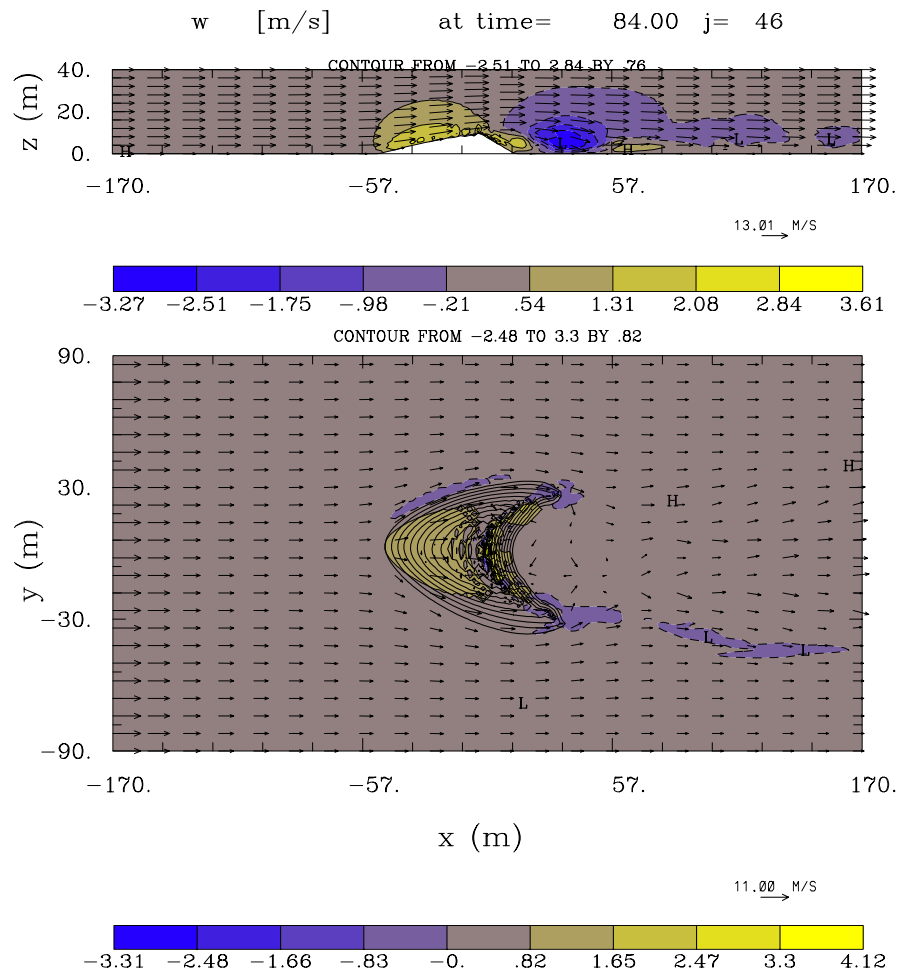


Figure 4: LES of PBL past a rapidly evolving sand dune

Simulations of boundary layer flows past sand dunes — $340 \times 180 \times 40 \text{ m}^3$ domain covered with $\delta x = \delta y = 2 \text{ m}$, $\delta z = 1 \text{ m}$ — depend on explicit SGS model (here TKE), because the saltation physics that controls dune evolution depends crucially on the boundary stress.

- DNS \Leftrightarrow TRUE, although limited to low Reynolds number flows, a useful complement of laboratory experiments.

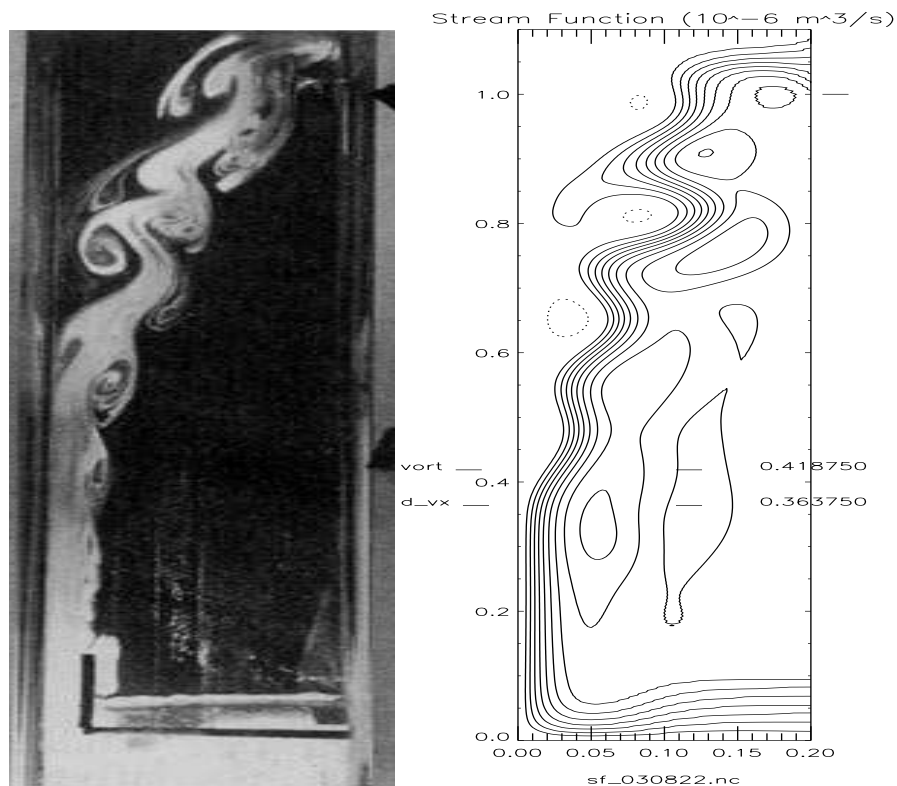


Figure 5: Baines & Hughes experiment (1996, JPO) vs. DNS

Simulations of the rotating tank experiment — $\beta = 0.091 f/H$; the $1.10 \times 0.20 \times 0.21 \text{ m}^3$ domain covered with $\delta x = \delta y = \delta z$: 0.01, 0.005, 0.0025 m — show convergence and produce simulation that agrees well with the laboratory result, enabling a model-based analysis of the physics of western boundary current separation.

Anelastic Model: Analytic Formulation

Prusa & Sm., JCP 2003; Wedi & Sm., JCP 2004

- *diffeomorphic* mapping (RE “ With mesh adaptivity for simulating complex geophysical flows in mind ...”)

$$(\bar{t}, \bar{x}, \bar{y}, \bar{z}) \equiv (t, E(t, x, y), D(t, x, y), C(t, x, y, z)) , \quad (1)$$

(t,x,y,z) does not have to be Cartesian!

- Anelastic system of Lipps & Hemler (*J. Atmos. Sci.*, 1982)

$$\frac{\partial(\rho^* \bar{v}^{sk})}{\partial \bar{x}^k} = 0 . \quad (2)$$

$$\frac{dv^j}{d\bar{t}} = - \bar{G}_j^k \frac{\partial \pi'}{\partial \bar{x}^k} + g \frac{\theta'}{\theta_b} \delta_3^j + \mathcal{F}^j + \mathcal{V}^j , \quad (3)$$

$$\frac{d\theta'}{d\bar{t}} = - \bar{v}^{sk} \frac{\partial \theta_e}{\partial \bar{x}^k} + \mathcal{H} , \quad (4)$$

$$\bar{v}^{sk} := \bar{v}^{*k} - \frac{\partial \bar{x}^k}{\partial t} ; \quad \bar{v}^{sj} = \bar{G}_k^j v^k . \quad (5)$$

$$\rho^* := \rho_b \bar{G} ; \quad d/d\bar{t} = \partial/\partial \bar{t} + \bar{v}^{*k} (\partial/\partial \bar{x}^k) ; \quad \bar{v}^{*k} := d\bar{x}^k/d\bar{t} := \dot{\bar{x}}^k$$

$$\bar{G}_j^k := \sqrt{g^{jj}} (\partial \bar{x}^k / \partial x^j) \iff ds^2 = g_{pq} dx^p dx^q , \quad g_{pk} g^{kq} \equiv \delta_p^q$$

Finite-Difference Approximations

Sm. & Prusa, in *Turbulent Flow Computation*, Kluwer, 2002

• Each prognostic equation can be written as either *Lagrangian* evolution equation or *Eulerian* conservation law:

$$\frac{d\psi}{d\bar{t}} = R \quad , \quad \frac{\partial \rho^* \psi}{\partial \bar{t}} + \bar{\nabla} \bullet (\rho^* \bar{\mathbf{v}}^* \psi) = \rho^* R . \quad (6)$$

$\psi \equiv v^j$ or θ' , and R the associated rhs, $\bar{\nabla} \bullet := (\partial/\partial \bar{x}, \partial/\partial \bar{y}, \partial/\partial \bar{z}) \bullet$.

• Either form is approximated to $\mathcal{O}(\delta t^2, \delta x^2)$

$$\psi_{\mathbf{i}}^{n+1} = LE_{\mathbf{i}}(\psi^n + 0.5\Delta t R^n) + 0.5\Delta t R_{\mathbf{i}}^{n+1} ; \quad (7)$$

where $\psi_{\mathbf{i}}^{n+1}$ is the solution sought at the grid point $(\bar{t}^{n+1}, \bar{\mathbf{x}}_{\mathbf{i}})$, LE denotes a two-time-level either advective semi-Lagrangian or flux-form Eulerian NFT transport operator (Sm. & Pudykiewicz, JAS, 1992; Sm. & Margolin, MWR 1993).

• (7) represents an algebraic system implicit for all $\psi \Rightarrow$ comments on formulating *elliptic* problem for π .

Anelastic Model: Analytic Formulation; Extensions

• VORTICITY

$$\bar{\omega}^*_{jk} = \bar{v}^*_{k,j} - \bar{v}^*_{j,k} \Rightarrow \omega^q = \varepsilon_{qjk} \sqrt{g^{kk}} \tilde{G}_j^p \frac{\partial \sqrt{g_{kk}} v^k}{\partial \bar{x}^p}; \quad (8)$$

in any system $\bar{v}^*_k = \bar{g}_{jk} \bar{v}^{*j}$, so in the physical space $v^*_j = \sqrt{g_{jj}} v^j$.

$$\nabla \bullet \boldsymbol{\omega} = \nabla \bullet \nabla \times \mathbf{v} \equiv 0 \Rightarrow$$

$$\frac{1}{G} \frac{\partial}{\partial \bar{x}^p} (\bar{G} \bar{\omega}^{sp}) \equiv 0, \quad \bar{\omega}^{sp} := \tilde{G}_p^q \omega^q. \quad (9)$$

Note the connection with the solenoidal velocity in (5)!

• SCALAR DIFFUSION

Defining Fickian flux $\Phi_j := \rho \alpha \phi_{,j}$ in the physical space $\Rightarrow \mathcal{L}(\phi) \Rightarrow$

$$\frac{\mathcal{D}\phi}{\mathcal{D}t} = S_\phi + \frac{1}{\rho^*} \frac{\partial}{\partial \bar{x}^j} \left(\alpha \rho^* \bar{g}^{jk} \frac{\partial \phi}{\partial \bar{x}^k} \right), \quad (10)$$

and, in particular,

$$\mathcal{H} = \frac{1}{\rho^*} \frac{\partial}{\partial \bar{x}^j} \left(\alpha \rho^* \bar{g}^{jk} \frac{\partial \theta'}{\partial \bar{x}^k} \right) \quad (11)$$

in the entropy equation (4).

• MOMENTUM DISSIPATION

From geometric principles in co-moving coordinates $\epsilon'_{jk} dx'^j dx'^k := 0.5\mathcal{D}/\mathcal{D}t' (ds'^2)$, via definition of the fundamental metric $\Rightarrow \epsilon'_{jk} \equiv 0.5\mathcal{D}/\mathcal{D}t' (g'_{jk})$, then transforming to $(\bar{t}, \bar{\mathbf{x}})$, expanding the *convected* derivative, and using Ricci's lemma ($\bar{g}_{jk,s} \equiv 0$) \Rightarrow

$$\bar{\epsilon}^*_{jk} \equiv \frac{1}{2} (\bar{v}^*_{k,j} + \bar{v}^*_{j,k}) , \quad (12)$$

the symmetric complement of the *rotation* (viz. $0.5\bar{\omega}^*_{jk}$ in Eq. (8)) to the gradient of the covariant velocity — the *objective* form.

To compute $\bar{\epsilon}^*_{jk}$, (12) is (i) written for physical space, (ii) the covariant derivatives expanded, (iii) the covariant velocities rescaled into the physical, and (iv) the derivatives rewritten in terms of transformed space \Rightarrow

$$\epsilon^*_{jk} \equiv \frac{1}{2} \left(\sqrt{g_{kk}} \tilde{G}_k^p \frac{\partial \sqrt{g_{jj}} v^j}{\partial \bar{x}^p} + \sqrt{g_{jj}} \tilde{G}_j^q \frac{\partial \sqrt{g_{kk}} v^k}{\partial \bar{x}^q} \right) - \sqrt{g_{mm}} \left\{ \begin{matrix} m \\ j \quad k \end{matrix} \right\} v^m .$$

Then, defining the deviatoric stress in terms of the strain rate in the physical space ($\rho_b \tau^{*jk} := 2\mu \epsilon^{*jk} + \lambda v^{*m}_{,m} \delta_k^j$) $\Rightarrow \mathcal{V}^j \equiv \sqrt{g_{jj}} \rho_b^{-1} (\rho_b \tau^{*jk})_{,k}$, the viscous term on the rhs of the momentum equation (3)

$$\mathcal{V}^j = \frac{1}{\rho^*} \frac{\partial}{\partial \bar{x}^p} \left(\rho^* \tilde{G}_k^p \sqrt{g_{jj} g_{kk}} \tau^{*jk} \right) - \tau^{*jk} \frac{\partial \sqrt{g_{jj}}}{\partial x^k} + \sqrt{g_{jj}} \left\{ \begin{matrix} j \\ l \quad m \end{matrix} \right\} \tau^{*lm} ;$$

$$\tau^{*jk} = 2\nu g^{jj} g^{kk} \epsilon^*_{jk} + \kappa g^{jk} v^{*m}_{,m} ; \quad \nu := \mu/\rho , \quad \kappa := \lambda/\rho . \quad (13)$$

• TENSOR IDENTITIES

$$\frac{\mathcal{D}\phi}{\mathcal{D}t} \equiv \frac{\partial\phi}{\partial x^q} v^q \equiv \frac{\partial\phi}{\partial \bar{x}^r} \frac{\partial \bar{x}^r}{\partial x^q} v^q \equiv \frac{\partial\phi}{\partial \bar{x}^r} \bar{v}^r =: \frac{\mathcal{D}\phi}{\mathcal{D}\bar{t}}. \quad (14)$$

$$\frac{D\bar{v}^{*j}}{D\bar{t}} := \bar{v}^{*j}_{,m} \bar{v}^{*m} \equiv \frac{d\bar{v}^{*j}}{d\bar{t}} + \overbrace{\left\{ \begin{matrix} j \\ i \ m \end{matrix} \right\}} \bar{v}^{*i} \bar{v}^{*m}. \quad (15)$$

$$\delta_s^r \equiv \frac{\partial \bar{x}^r}{\partial x^q} \frac{\partial x^q}{\partial \bar{x}^s}. \quad (16)$$

$$\frac{G}{\bar{G}} \frac{\partial}{\partial \bar{x}^r} \left(\frac{\bar{G}}{G} \frac{\partial \bar{x}^r}{\partial x^s} \right) \equiv 0. \quad (17)$$

Examples

- Flapping membranes (Wedi & Sm., *JCP*, 2004)

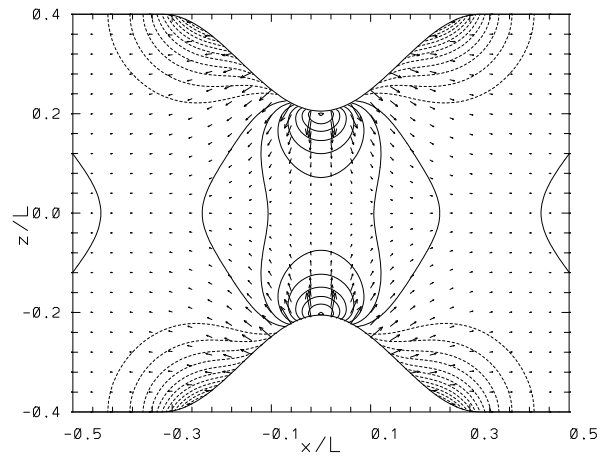


Figure 6: Potential flow simulation past 3D undulating boundaries

Table 1: Vorticity errors in a potential flow simulation

field	Max $ \cdot $	Average	Standard deviation
$\Delta t \omega^1$	$6.99 \cdot 10^{-2}$	$-4.87 \cdot 10^{-18}$	$1.90 \cdot 10^{-3}$
$\Delta t \omega^2$	$6.98 \cdot 10^{-2}$	$-3.19 \cdot 10^{-17}$	$1.90 \cdot 10^{-3}$
$\Delta t \omega^3$	$7.62 \cdot 10^{-3}$	$2.20 \cdot 10^{-18}$	$1.71 \cdot 10^{-4}$
$\Delta t \nabla \bullet \omega^s$	$2.94 \cdot 10^{-5}$	$-7.52 \cdot 10^{-18}$	$3.75 \cdot 10^{-7}$

- Mesoscale valley flows

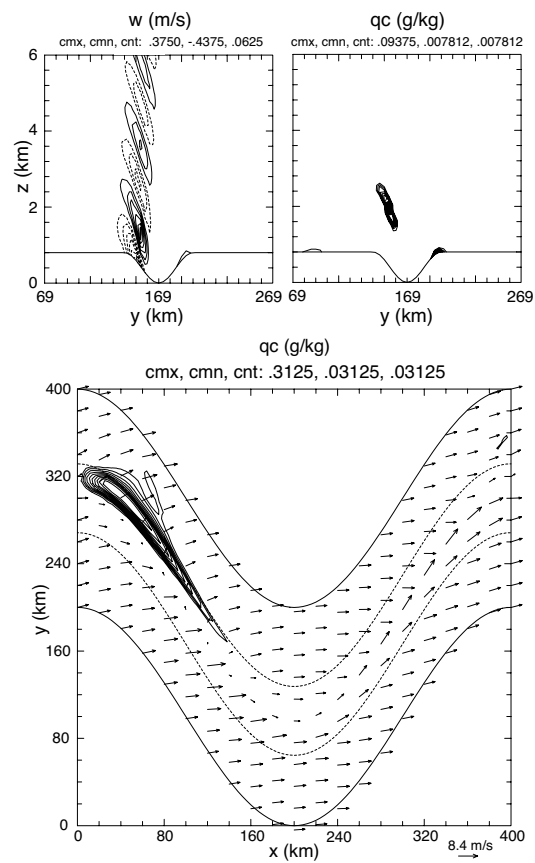


Figure 7: Vertical velocity (outer left panel) and cloud water mixing ratio (inner left panel) in the yz cross section at $x = 120$ km and cloud-water mixing ratio at bottom surface of the model (right panel).

Examples of Useful Transformations

- Analytic approach

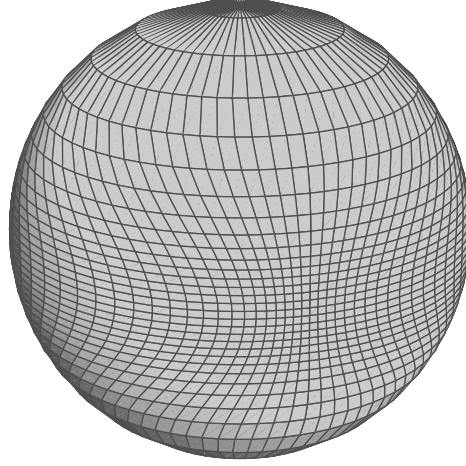


Figure 8: Continuous global mesh transformation, an example

$$Y(\bar{t}, \bar{Y}) = S_y^{-1} \bar{Y} + (1 - S_y^{-1}) \bar{Y}^n, \quad (18)$$

$$X(\bar{t}, \bar{X}, \bar{Y}) = F_0(\bar{Y}) \cdot X_0(\bar{t}, \bar{X}) + F_1(\bar{Y}) \cdot \bar{X} + T(\bar{t}). \quad (19)$$

$\bar{X} \in [0, 1]$ and $\bar{Y} \in [-1, 1]$ are normalized \bar{x} and \bar{y} . The auxiliary functions

$$F_0(\bar{Y}) = (1 - \bar{Y}^2), \quad F_1(\bar{Y}) = 1 - F_0(\bar{Y}), \quad (20)$$

$$X_0(\bar{t}, \bar{X}) = [S_x^{-1} + (1 - S_x^{-1}) \cdot f(\bar{X})] \cdot \bar{X}, \quad (21)$$

assume $f(s) = (10 - 15s + 6s^2) \cdot s^2$ with S_x^{-1}, S_y^{-1} in the form $S^{-1}(\tau) = S_i^{-1} + (S_f^{-1} - S_i^{-1}) \cdot \tau \cdot f(\tau)$, for $\tau = (\bar{t} - \bar{t}_i) / (\bar{t} - \bar{t}_f) \in [0, 1]$, and S_i^{-1}, S_f^{-1} denote the initial and final values of maximum stretch occurring at times \bar{t}_i, \bar{t}_f , respectively; for $\tau \notin [0, 1]$, $S^{-1} = \text{const.}$; $T(\bar{t})$ in (19) allows zonal translation. Figure 8 is at the time when $S_x \equiv 3$ and $S_y \equiv 3$ in (18)-(21), with $n = 5$.

- Discrete approach

The mesh evolution is postulated via ‘mesh-continuity’ equation:

$$\frac{\partial \delta_x}{\partial \bar{t}} + \frac{\partial U \delta_x}{\partial \bar{x}} = 0. \quad (22)$$

where $\delta_x = \delta_x(\bar{t}, \bar{x})$ is the physical-grid-increment function of the transformed coordinates, proportional to a finite difference representation of a grid stretching factor $\partial x / \partial \bar{x}$.

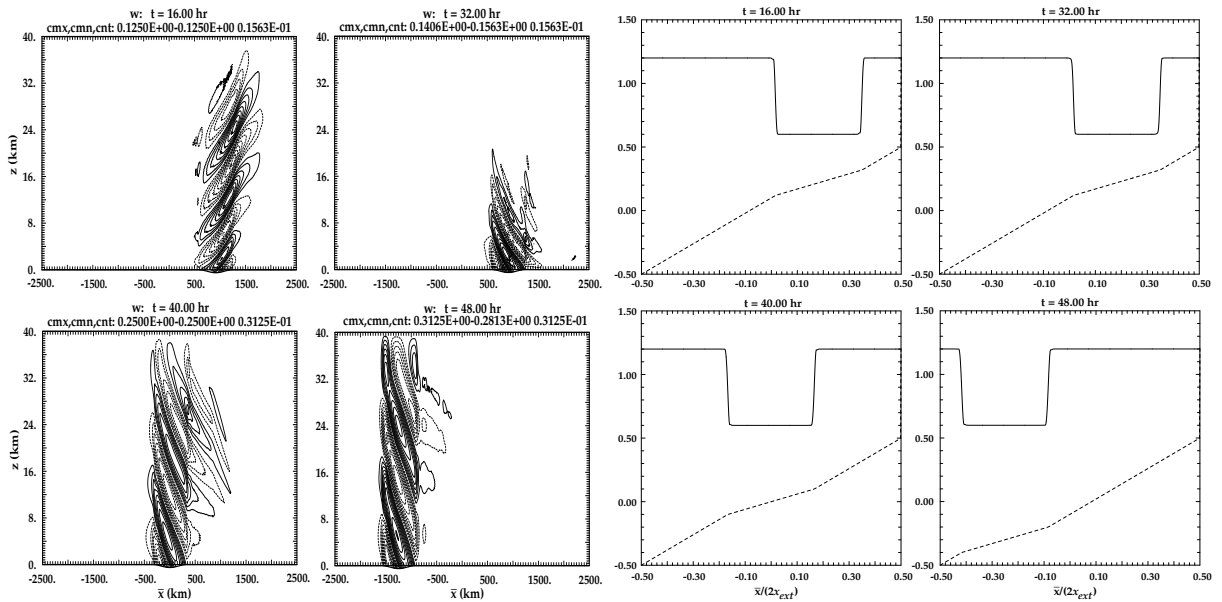


Figure 9: Traveling inertia-gravity wave packet, Prusa & Sm., JCP 2003; grid stretching factor $\delta_x / \Delta \bar{x}$ (solid line) and physical coordinate $x(\bar{t}, \bar{x})$.

Remarks

- We admit any orthogonal and stationary (curvilinear, in particular) coordinate system for the physical domain. This is a significant departure from earlier transformation methods, which are limited to Cartesian descriptions of the physical space (and has required re-derivation of all relevant physical forms).
- While in principle one can always transform from Cartesian coordinates to any other topologically equivalent coordinates, in practice it is easier and more illuminating to use an established reference system that points out the obvious physics, e.g., spherical coordinates for global problems.
- By limiting (t, \mathbf{x}) to orthogonal and stationary, we take advantage of important simplifications (i.e., compact scale factors and reduced index range in many operators) that are unavailable, if the problem were to be cast in an arbitrary curvilinear framework.
- We depart from most computational works in emphasizing a tensorial description of the model. We find this helpful for (i) generating correct and meaningful computational forms in arbitrary coordinates, and (ii) developing fundamental structure in the core of the numerical model that aids preserving local as well as global conservation properties.
- We find NFT numerical methods beneficial for computations on dynamically deforming grids. For example, robust performance of NFT methods allows to mimic moving nests with abruptly changing grid resolution.